

Journal of Materials Chemistry C

Accepted Manuscript



This is an *Accepted Manuscript*, which has been through the Royal Society of Chemistry peer review process and has been accepted for publication.

Accepted Manuscripts are published online shortly after acceptance, before technical editing, formatting and proof reading. Using this free service, authors can make their results available to the community, in citable form, before we publish the edited article. We will replace this *Accepted Manuscript* with the edited and formatted *Advance Article* as soon as it is available.

You can find more information about *Accepted Manuscripts* in the [Information for Authors](#).

Please note that technical editing may introduce minor changes to the text and/or graphics, which may alter content. The journal's standard [Terms & Conditions](#) and the [Ethical guidelines](#) still apply. In no event shall the Royal Society of Chemistry be held responsible for any errors or omissions in this *Accepted Manuscript* or any consequences arising from the use of any information it contains.

Cite this: DOI: 10.1039/c0xx00000x

www.rsc.org/xxxxxx

ARTICLE TYPE

Alkyl-triphenylamine End-capped Triazines with AIE and Large Two-photon Absorption Cross-sections for Bioimaging

Yuting Gao^a, Yi Qu^b, Tao Jiang^a, Hao Zhang^a, Nannan He^a, Bo Li^c, Junchen Wu^{a*}, and Jianli Hua^{a*}

Received (in XXX, XXX) Xth XXXXXXXXX 20XX, Accepted Xth XXXXXXXXX 20XX

DOI: 10.1039/b000000x

Three new luminogens **ATT-(1–3)** based on 1,3,5-triazine and end-capped with multi-branched triphenylamine containing alkyl chain have been synthesized and characterized. All the three dyes are nonemissive in solution but strong red fluorescent emission in aggregate state. The two-photon absorption (2PA) cross sections measured by the open aperture Z-scan technique are determined to be as large as 2756, 4750 and 10003 GM for **ATT-1**, **ATT-2** and **ATT-3** in chloroform, respectively, which show a dramatic enhancement with increasing number of donor branches. The relationship between their structures and properties on one- and two-photon absorption and aggregation-induced emission (AIE) is discussed, which can serve as a guideline for the development of a series of solid materials with larger two-photon cross section and high fluorescent quantum yield. In addition, one- and two-photon fluorescence (2PF) microscopy images of HeLa cells incubated with these three dyes are carried out to exploit the potential applications of these fluorophores in biosensing and bioimaging.

Introduction

Two-photon absorption (2PA) is a way of accessing a given excited state by using photons of twice the wavelength of the corresponding one-photon absorption, which increases with the square of the light intensity. 2PA materials have various superiorities, such as deep penetration, high three-dimensional spatial selectivity and negligible background fluorescence, arousing considerable interest as promising materials for applications in various areas, such as two-photon dynamic therapy, three-dimensional optical data storage, up-converted lasing, optical power limiting materials, two photon microscopy and bioimaging.¹ Nowadays, two-photon laser scanning fluorescence microscopes are commercially available and become common tools for biologists, which have generated an imperative demand for new dyes with high 2PA cross-sections (σ) and highly fluorescence output.² As most conventional dyes have only modest σ and short emissive wavelength, how to synthesize large σ materials has become a significant issue.³ The strategy for the design of molecules with large σ has provided guidelines for the development of 2PA materials, including dipolar, quadrupolar and octupolar molecule and other archetypes.⁴ The accumulated knowledge and experience has revealed that the value of σ is correlated with intramolecular charge transfer. Moreover, the large conjugation length of π system with enforced coplanarity, the modification of donor/acceptor groups and branching symmetry are efficient design strategies for large σ value.⁵ Currently, many 2PA materials with multibranched triarylamine have been synthesized for their good electron-donating and transporting capabilities, which can enhance the 2PA performance owing to the increase in π -electron density of the system.⁶

However, according to the strategy, many materials synthesized with large 2PA cross-sections are in enforced

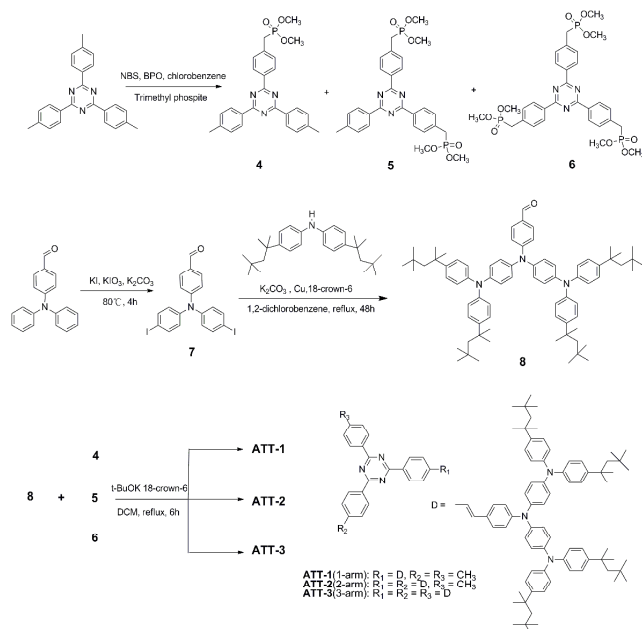
coplanarity structure and conformational rigidity. Most of these compounds are hydrophobic and their fluorescence quantum yields are considerably reduced in water on account of the aggregation of molecules, which generally leads to fluorescence quenching.⁷ The shortcoming, which is notoriously known as aggregation-caused quenching (ACQ), seriously limits their applications, especially in fluorescent chemosensors and bioimaging. Hence, a special molecular design for 2PA materials is required not only to ensure large two-photon activity, but more importantly, to overcome fluorescence quenching at high concentration. In 2001, Tang and his coworkers discovered a group of silole-based anti-ACQ materials, called aggregation-induced emission (AIE) compounds.⁸ The AIE molecules are nonemissive when dissolved in good solvents but become highly luminescent when aggregated in the solid state. They also developed a series of AIE luminogens and identified restriction of intramolecular rotation (RIR) and twisted intramolecular charge transfer (TICT) in the aggregates as main causes for the AIE effect through experimental and theoretical studies.⁹ Now AIE luminogens have showed significant academic value and diverse promising applications in cell imaging,¹⁰ fluorescent sensors and bioprobes,¹¹ mechanofluorochromic materials.¹² As far as we known, large works on the AIE fluorophores for bioapplications are focused on TPE species with shorter wavelength input and output signals.¹³ Consequently, there are still very necessary to develop the long wavelength emission AIE materials with large 2PA cross section for bioapplications.

Previously, our group reported a 1,3,5-triazine based 2PA chromophore combined with AIE property, **TAPA-a**, which was fabricated into nanoparticles with PEG and used for cancer cell imaging successfully.¹⁴ Although the energy of the IR light is lower than the visible light, the strong excitation can still induce damages to the samples and bleaching of the dyes. Thus there is a strong need of dedicated fluorophores with higher σ to keep the laser power as low as possible, in order to avoid too high peak

powers in the excitation volume.¹⁵ In this work, we have induced multiple alkyl chains into the large π system and synthesized polynuclear aromatic amine branched compounds **ATT-(1-3)** with larger σ and higher quantum yields. Furthermore, sonication-assistant nanoparticle fabrication was used in this study and these materials can be fabricated into nanosphere without PEG coat. Different number of branches attached on the 1, 3, 5-triazine were used to study the relationships between structure and photophysical properties. As expected, an improvement of the 2PA cross-section was observed for the three new structures, which involved linkage of one-, two- or three-triphenylamine branch(s) through a common triazine core group. In particular, the starburst **ATT-3** comprised of 1,3,5-triazine core and six electron-donating alkyl-diphenylamines linked by π -conjugated bridge shows extraordinary large σ of 10031 GM, which is larger than that of **TAPA-a** without long alkyls (8629 GM). Further study on the bioapplication showed that these three materials were all suitable for cell imaging that performed by both one-photon and two-photon laser scanning confocal microscopy.

Result and discussion

Synthesis



Scheme 1 Synthetic routes to the **ATT**-based compounds

The targeted compounds **ATT-(1-3)** were synthesized according to Scheme 1. Bromination of 2,4,6-tri(p-tolyl)-1,3,5-triazine afforded 2-(4-(bromomethyl)phenyl)-4,6-di-p-tolyl-1,3,5-triazine, 2,4-bis(4-(bromomethyl)phenyl)-6-(p-tolyl)-1,3,5-triazine and 2,4,6-tris(4-(bromomethyl)phenyl)-1,3,5-triazine, followed by reaction with trimethyl phosphate, yielding triazine derivatives **4**, **5** and **6**. The important intermediate aldehyde **8** was synthesized by Ullmann reaction from triphenylamine aldehyde iodide **7** and bis(4-tert-octylphenyl)amine. Finally, condensation of aldehyde **8** with the respective triazine moiety (**4**, **5**, **6**) by the Horner–Wadsworth–Emmons reaction gave the target compounds **ATT-(1-3)**.

All compounds were purified by column chromatography or recrystallization and characterized by ¹H NMR, ¹³C NMR and mass spectra (shown in ESI).

Photophysical Properties

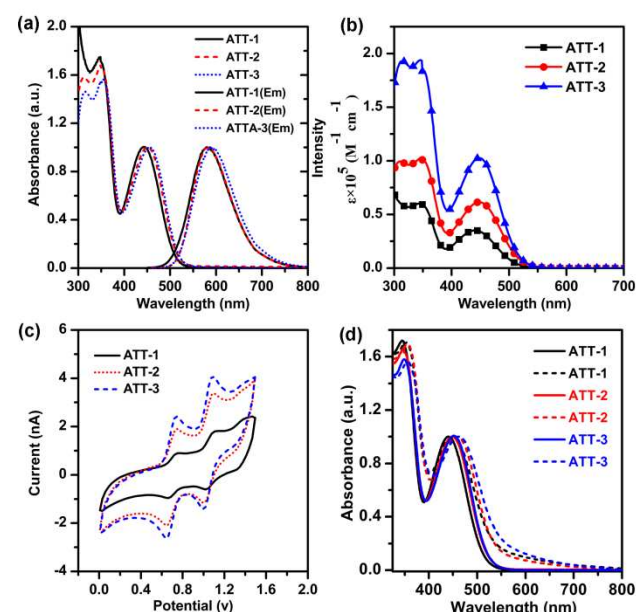


Fig. 1 (a) Normalized absorption and emission spectra of **ATT-(1-3)** in toluene at room temperature at 1×10^{-5} M. (b) Absolute absorption spectra of **ATT-(1-3)** in THF at 1×10^{-5} M. (c) Cyclic voltammogram of **ATT-(1-3)** in DCM. (d) Normalized one-photon absorption of **ATT-(1-3)** in THF (solid line) and in dispersion of the nanoaggregate form (90% water) (dashed line) at 1×10^{-5} M.

Fig. 1 (a) shows the steady-state absorption and emission spectra of **ATT-(1-3)** in toluene at 298 K. All these chromophores exhibit intense linear absorption in the UV/Vis region with the lowest-energy peaks located at 447, 450, 453 nm, respectively, which is slightly red-shifted by increasing number of branches. The fluorescence peaks are nearly identical at 594, 598, 602 nm for **ATT-(1-3)**, showing a large Stokes shift of 147, 148 and 149 nm, respectively. The similar behavior is observed for other solvents, shown in Table 1. However, the extinction coefficient is strictly proportional to number of branches, being increased from 3.3×10^4 $M^{-1}cm^{-1}$ in **ATT-1** to a doubled value of 6.1×10^4 $M^{-1}cm^{-1}$ in **ATT-2** and a tripled number of 1.0×10^5 $M^{-1}cm^{-1}$ for **ATT-3** at peak wavelength in THF, as shown in **Fig. 1**(b). This is contributed to the independent of number of branch in **ATT-(1-3)**, the lowest lying excitation is mainly localized on a specific arm, which is demonstrated in our previous work.¹⁶ Interestingly, the emission maximum (λ_{em}) of **ATT-1** shifts correspondingly from 594 to 675 and to 682 nm when the solvent polarity is increased from toluene to THF and to DCM. The similar phenomenon is observed in the solutions of **ATT-2** and **ATT-3** (Table 1). In this case, the quantum yields (Φ) of emission of **ATT-(1-3)** decrease with increasing solvent polarity. The cause of the solvent effect is that the **ATT-(1-3)** derivatives are comprised of triphenylamine donor (D) and triazines acceptor (A) units. Such D-A molecules often show solvatochromic effects, which has been well explained by a twisted intramolecular charge transfer (TICT)

mechanism.¹⁷ Elevation of the HOMO level in TICT state narrows the band gap thereby red-shifting the emission spectrum. However, its emission intensity is weakened because of the susceptibility of the TICT state to various nonradiative quenching processes. Therefore, **ATT-(1-3)** shows a relatively high Φ value in a nonpolar solvent toluene. In addition, the electrochemical behavior of **ATT-(1-3)** was investigated by cyclic voltammetry using 0.1 M tetrabutylammonium hexafluorophosphate as supporting electrolyte in dichloromethane solution with platinum button working electrodes, a platinum wire counter electrode, and an SCE reference electrode. The SCE reference electrode was calibrated using a ferrocene / ferrocenium (Fc/Fc⁺) redox couple as an external standard. It is shown in Fig. 1(c) that all the three compounds exhibit the first oxidation peak in the region of 0.69 V. The result reveals that the electron density is located in a single arm, consistent with the conclusion drawn from the absorption measurement.

Table 1 Photophysical Properties of **ATT-(1-3)** at 298 K.

	Solvent	$\lambda_{\text{abs}}(\text{nm})$ ($\epsilon \times 10^{-4}$ $\text{M}^{-1}\text{cm}^{-1}$)	λ_{em} (nm)	QY, Φ^b	Emission decay(ns) (A_1, A_2)	K_{rad} (10^8 s^{-1}) ^c
ATT-1	toluene	447 (3.0)	594	0.79	3.1	2.5
	THF	441 (3.3)	675	0.0081	0.090	0.29
	DCM	443 (3.2)	682	0.0019	<0.050	0.83
	H ₂ O/ THF ^a	448	592	0.04	2.3, 9.7 (0.62, 0.38)	-
	ATT-2	toluene	450 (5.8)	598	0.69	2.9
THF	449 (6.1)	676	0.0091	0.11	0.83	
DCM	447 (6.3)	693	0.0013	<0.050	0.46	
H ₂ O/ THF ^a	458	596	0.21	2.6, 10.1 (0.45, 0.55)	-	
ATT-3	toluene	453 (10.0)	602	0.65	2.8	2.3
	THF	452 (10.2)	678	0.0073	0.11	0.66
	DCM	453 (10.9)	695	0.0011	<0.050	0.48
	H ₂ O/ THF ^a	462	599	0.27	3.2, 11 (0.37, 0.63)	-

^a H₂O/THF (9:1). ^b The PL quantum yield (Φ) was estimated with rhodamine B in ethanol as a standard. ^c K_{rad} : radiative decay rate constant. The rate constants for radiative decays can be estimated from the fluorescence quantum yields and lifetimes according to reference.¹⁸

All the **ATT**-based derivatives are soluble in common organic solvents such as THF, toluene and DCM but are insoluble in water. Stable water dispersions of **ATT**-based nanoaggregates were prepared by the precipitation method using THF as a water-miscible solvent for dyes. Fig. 1(d) shows the normalized one-photon absorption of **ATT-(1-3)** in THF and in dispersion of the aggregate form (90% water) at 1×10^{-5} M. The absorption maxima (λ_{max}) of them were appearing at 441, 449 and 452 nm in THF, respectively. The absorption of **ATT-(1-3)** in dispersion of the

aggregate form (90% water) was obviously broadened and their λ_{max} moved to 448, 458, 462 nm, which was bathochromically shifted by 7, 9, 10 nm, respectively. The absorption spectra of **ATT-(1-3)** were broadened, implying that the molecular stacking is well ordered within the nanoaggregated structure. The absorption tails extending well into the long wavelength region further indicated the luminogens' aggregation into particles in the presence of water, as it is well known that the Mie effect of particles causes such level-off tails in the absorption spectra.¹⁹

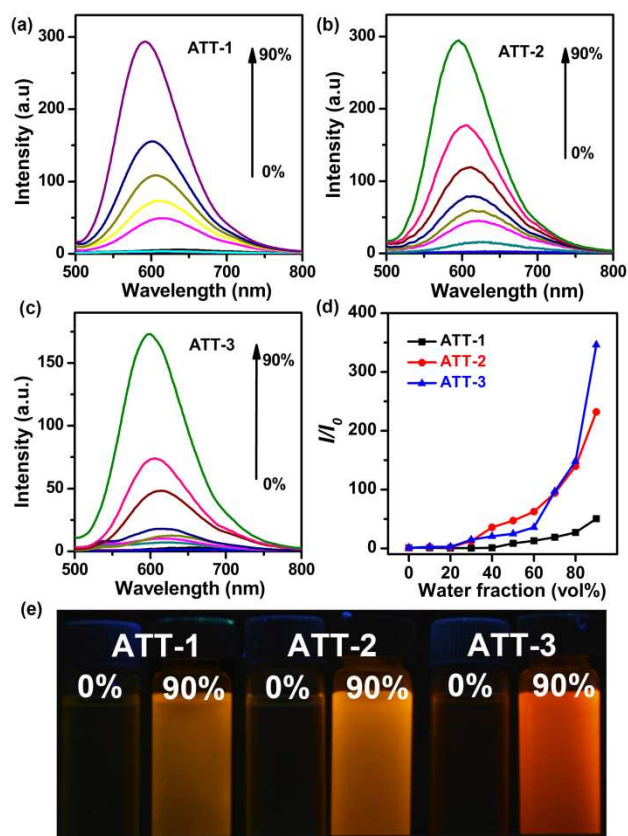


Fig. 2 (a, b, c) Corresponding emission spectra of compound **ATT-(1-3)** in THF-water mixtures with different water fraction at 1×10^{-5} M. Excitation wavelength: 450 nm. (d) Plot of I/I_0 vs water content of the solvent mixture, where I_0 is the PL intensity in pure THF solution. (e) Photographs of **ATT-(1-3)** in the pure THF solution and in 90% water-THF mixture taken under illumination of a UV light.

The corresponding emission spectrum of **ATT-1** is shown in Fig. 2 (a) in aqueous THF with different water/THF ratios at 1×10^{-5} M. The emission from the THF solution of **ATT-1** was so weak that almost no photoluminescence (PL) signal was recorded. However, an obvious enhancement of luminescence was observed at the 40% (v/v) water-THF mixture and the PL signal was gradually enhanced with the increasing water/THF ratios. While the water/THF ratio reached to 90 %, the PL intensity boosted to the maximum. Since **ATT-1** was insoluble in water, **ATT-1** nanoparticles began to aggregate with increasing of water fraction. The aggregated particles restricted intramolecular rotation (RIR) process and thus facilitated the radiative decay of the excitons, making the luminogen fluoresce strongly. The similar behavior was observed for **ATT-2** and **ATT-3** in Fig. 2 (b, c), verifying that the three luminogens were AIE-active.

Moreover, the PL emissions of the luminogens were slightly blue-shifted with increasing water content, which could be contributed to its parallel packing mode. To demonstrate the PL intensity changes of the compounds more visually, we plotted the changes in their PL peak intensities (I/I_0) versus water content of mixture as shown in Fig. 2 (d). The PL intensity of **ATT-(1-3)** in THF solution was very low and almost unchanged when water ratio was added up to 40%, 20% and 20% (v/v), respectively, but started to increase swiftly upon addition of water to 50%, 30% and 70% (v/v), respectively. While the water/THF ratio reached to 90%, they emitted strongly orange luminescence with 50-fold, 232-fold and 346-fold increase in the I/I_0 ratio, respectively. The AIE effect is enhanced with increasing the number of branch arms. The fluorescence behavior of **ATT-(1-3)** is well visualized through fluorescence images of solution and aggregate dispersions as shown in Fig. 2 (e).

To get insight into the possible mechanism of AIE, time-correlated single photon counting method (TCSPC) was used to elucidate the fluorescence decay of **ATT**-based compounds in THF and the THF–water mixture solution (v/v = 1:9). As can be seen from Table 1 that the fluorescence of the **ATT-3** in THF solution decays very fast, and is well-fitted by single exponential decay with emission lifetime as short as ~110 ps. It can be inferred that intramolecular vibrational and torsional motions can

act as efficient nonradiative pathways for the excited states to decay. The fluorescence lifetime data for **ATT-3** in the mixture containing 90% water are also given, which were obtained by fitting the time-resolved fluorescence curves based on the following double-exponential function:²⁰

$$Y = A_1 e^{-t/\tau_1} + A_2 e^{-t/\tau_2}$$

Fitting based on this function gave better fitting results than that on the single-exponential function for the sample with water. The molecules in the mixed solvent are suspected to exist in two different environments, or decay through two relaxation pathway. The values of A_1 and A_2 represent the fractional amount of molecules in two different environments. In 90% water–THF mixture solution, the fluorescence decay curve is well-fitted biexponentially with a decay time constant of ~3.2 ns (0.37) and a rather long decay time constant of ~11 ns (0.63). It is suggested that the nanosecond decay components are attributed to the emission from formation nanostructure which restricts the rotation of the molecular. The similar behavior was observed for **ATT-1** and **ATT-2**. What is more, the percentage of the molecule having a long decay gets higher with increasing the number of branches, which can be contributing to high quantum yields.

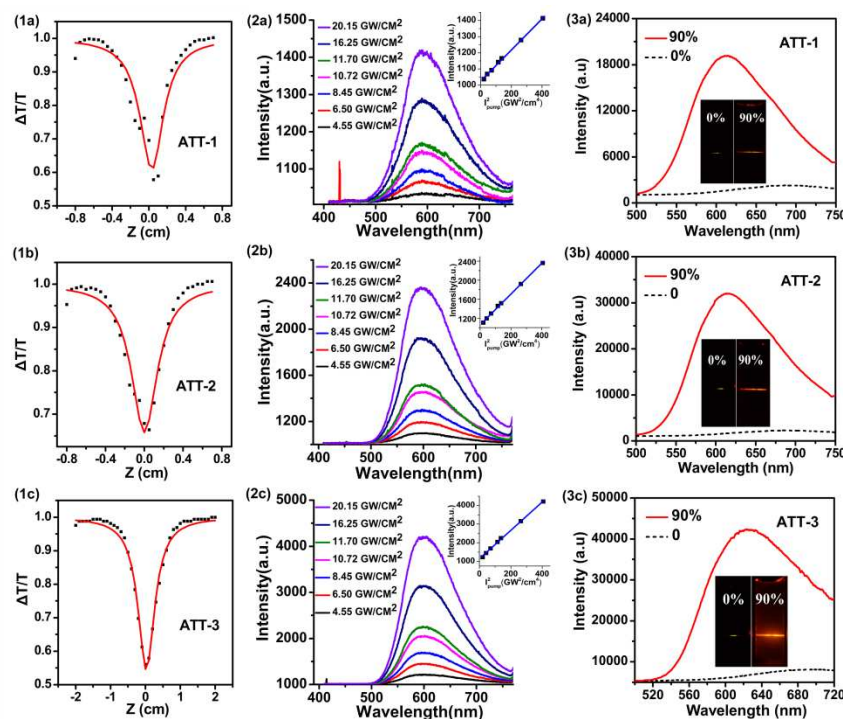


Fig. 3 (1a-1c) Open-Aperture Z-scan trace of **ATT-(1-3)** (scattered circle experimental data, straight line theoretic fitted data). (2a-2c) 2PF intensities of **ATT-(1-3)** under different excitation power density in toluene, respectively. Inset: 2PF intensity versus the square of the excitation power density. (3a-3c) Two-photon fluorescence emissions spectra and 2PA emissions images for **ATT-(1-3)** in solution (THF) and in dispersion of the nanoaggregate form (90% water) at 1×10^{-5} M, excited at 800 nm. **ATT-1**: 1a-3a; **ATT-2**: 1b-3b; **ATT-3**: 1c-3c

Two-Photon Absorption Properties

2PA cross sections of the **ATT-(1-3)** were determined by femtosecond open aperture Z-scan technique. Fig. 3 (1a-1c) shows the open-aperture Z-scan data and 2PA coefficient got by

data fitting. The σ can be calculated by using the equation of $\sigma = h\nu\beta N_0$, where $N_0 = N_A C$ is the number density of the absorption centers, N_A is the Avogadro constant and C represents the solute molar concentration. The values of σ for **ATT-(1-3)** are 2756, 4750 and 10003 GM at wavelength of 800 nm, respectively. A steeper increase in the σ value (1: 1.7: 3.6) was observed with

number of donor branches which extended conjugation of the molecular structure. It is well known that increasing the number of conjugation paths or connecting several linear paths to form a two-dimensional (2D) or three-dimensional (3D) configuration has shown theoretically and experimentally to be able to increase 2PA responses.²¹ In addition, the eight terminal octyl chains have improved the electron-donating ability and solubility of ATT-3, which results in a considerable increase in the value of 2PA cross section compared to compound TAPA-a.²² The two photon fluorescence spectrum of the three compounds under different laser intensity is shown in Fig. 3 (2a-2c). The linear dependence of fluorescence intensity on the square of the excitation intensity as shown in the inset confirms that 2PA is the main excitation mechanism of the intense fluorescence emission.

Under the excitation of 80 fs, 800 nm pulse, ATT-(1-3) in a mixture of THF and water emit intense fluorescence with the peaks located at 611 nm, 614 nm and 625 nm (Fig. (3a-3c)), respectively. The two-photon excitation fluorescence is slightly red-shifted comparing with one-photon excitation on account of reabsorption of partial emissive fluorescence. The overlap between one- and two-photon excitation fluorescence indicates that the emissions resulted from the same excited state, regardless of the different mode of excitation. It shall be noted that the studied three chromophores have performed two-photon excitation studies at one wavelength (800 nm). As the photos shown in Fig. 4, two-photon fluorescence (2PF) was remarkably intensified by aggregation in 90% water-THF mixture.

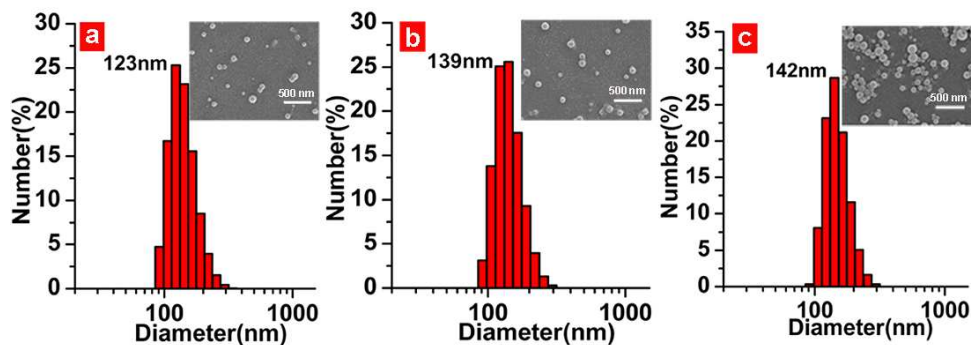


Fig. 4 Particle size distribution of ATT-1(a), ATT-2(b), ATT-3(c) in water studied via DLS and SEM (inserted images)

Preparation of ATT-(1-3) nanoparticles and cellular imaging

ATT-(1-3), with exceptional AIE and 2PA capacities, were selected to perform one- and two-photon fluorescence microscopy imaging. The size distribution of the ATT-(1-3) nanoparticles (NPs) was studied by using dynamic light scattering (DLS). As shown in Fig. 4, the mean diameter for these three dyes in water was approximately 123, 139 and 142 nm, respectively. Scanning electron microscopy (SEM) was also performed to study the morphology of the nanoparticles. The nanoparticles in SEM image have an average diameter of around 100, 110 and 120 nm, respectively, which is slightly smaller than those in DLS. This is because of the shrinking of samples when transformed into a dry state from solution.²³

To demonstrate the applicability of ATT-(1-3) in cellular imaging, the bioimaging experiments were carried out by confocal laser scanning microscopy (CLSM) using HeLa cells as an example. The HeLa cells were incubated with PBS solution (pH = 7.4) of ATT-(1-3) (1 $\mu\text{g}/\text{mL}$) for 2 h at 37 $^{\circ}\text{C}$, which was shown in Fig. 5. Obviously, all the three dyes can work well as fluorescent emitters for bioimaging. ATT-(1-3), with exceptional AIE and 2PA capacities, were selected to perform two-photon fluorescence microscopy imaging, images of which were shown in Fig. 6. The fluorescent signal from cytoplasm is clearly observed, indicating that both ATT-(1-3) can serve as promising two-photon fluorescent biomaterials. In addition, the toxicity of ATT-(1-3) for HeLa cells was measured by using a standard MTT assay (Fig. 7). After HeLa cells were cultured with ATT-(1-3) (80 μM) in PBS at 37 $^{\circ}\text{C}$ for 24 h, the metabolic viability of HeLa cells were estimated to be no less than 80%. Hence, ATT-(1-3) has good biocompatibility with low cytotoxicity.

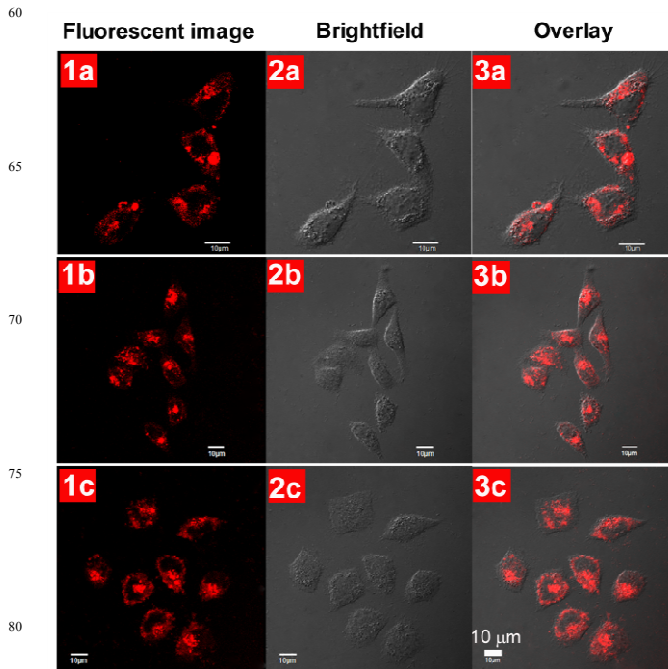


Fig. 5 CLSM images of HeLa cells after incubation with ATT-1(1a-3a), ATT-2(1b-3b) and ATT-3(1c-3c) NPs for 2 h at 37 $^{\circ}\text{C}$. Excitation at 488 nm. Fluorescence collection from 560 to 660 nm. The scale bar is 10 μm .

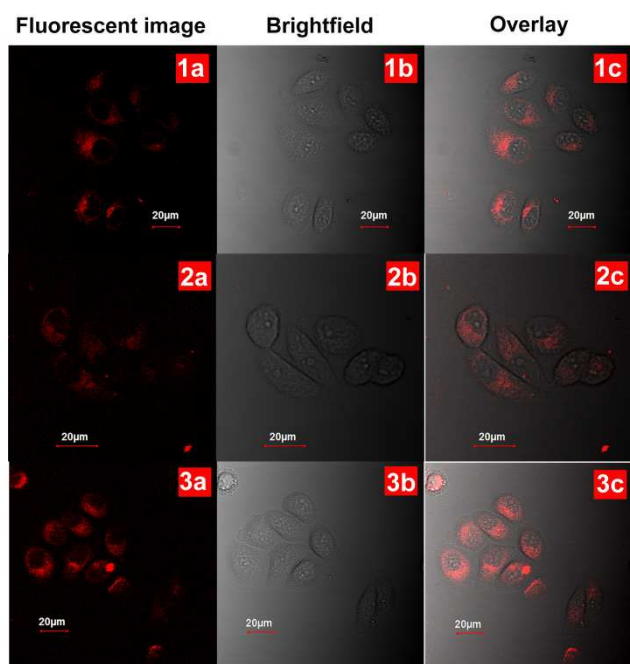


Fig. 6 Two-photon excited fluorescence imaging of HeLa cells after 1.5 h incubation with ATT-1(1a-3a), ATT-2(1b-3b) and ATT-3(1c-3c) NPs at 37 °C. The images were recorded upon 800 nm excitation with 560–660 nm band pass filter. (1a-3a) Two-photon excited fluorescence, (1b-3b) Brightfield and (1c-3c) Two-photon excited fluorescence/brightfield overlay. The scale bar is 20 μm.

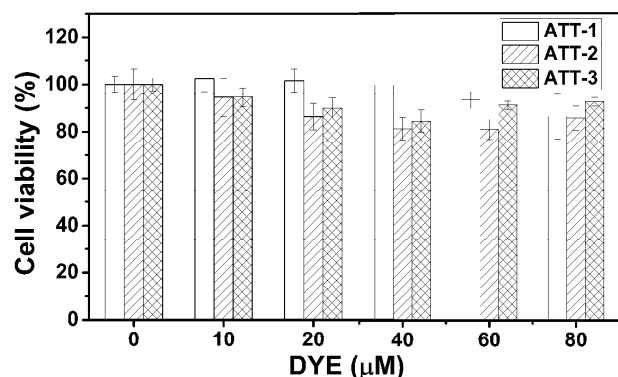


Fig. 7 Cell viability values (%) estimated by MTT proliferation test at 10 different concentrations of ATT-(1–3). HeLa cells were cultured in the presence of ATT-(1–3) at 37 °C for 24 h, respectively.

Conclusions

Both two-photon fluorescence and aggregation induced emission are powerful tools for biosensing and bioimaging fields. In this work, we have synthesized three new triazine-based chromophores with larger 2PA cross sections and brightness AIE fluorescence in water which contained different number of alkyl-triphenylamine as arms. As evidenced by TCSPC, intramolecular vibrational and torsional motions can act as efficient nonradiative pathways for the excited states to decay in THF solution making emission lifetime very short. In the contrary, fluorescence decay is slowed down a lot due to the restriction of intramolecular motions in aggregate state. In addition, the AIE effect is enhanced

with increasing the number of branches. More importantly, the two-photon absorption cross-sections of ATT-(1-3) can reach as large as 2756, 4750 and 10003 GM at wavelength of 800 nm in chloroform, respectively, which shows a great enhancement in the σ value with increasing number of donor branches. Furthermore, one- and two-photon fluorescent imaging was performed by confocal laser scanning microscopy and ATT-3 with the largest σ value showed as a potential material for bioapplications.

Experimental Section

Materials and Measurements

Tetrahydrofuran (THF) was pre-dried over 4 Å molecular sieves and distilled under argon atmosphere from sodium benzophenone ketyl immediately prior to use. *N, N*-dimethyl formamide (DMF) and dichloromethane (DCM) were refluxed with calcium hydride and distilled before use. Starting materials 2, 4, 6-Tri(*p*-tolyl)-1, 3, 5-triazine and 4-(diphenylamine)benzaldehyde were prepared according to published procedures.²⁴ All other chemicals were purchased from Aldrich and used as received without further purification.

¹H and ¹³C NMR spectra were recorded on a Bruker AM-400 spectrometer using chloroform-*d* (CDCl₃), tetrahydrofuran-*d*₈ (THF-*d*₈) or dimethylsulfoxide-*d*₆ (DMSO-*d*₆) as solvent and tetramethylsilane ($\delta = 0$) as internal reference. The UV/Vis spectra were recorded on a Varian-Cary 500 spectrophotometer with 2 nm resolution at room temperature. The fluorescence spectra were taken on a Varian-Cary fluorescence spectrophotometer. Time-resolved fluorescence measurement in this study was performed using the Edinburgh OB 900-L time-correlated single photon counting system (TCSPC). Emission was collected at right angle with respect to the pump. After deconvolution from the system response function, a temporal resolution of ~30 ps can be reliably obtained. The 2PA cross sections of ATT-(1–3) were measured by femtosecond open-aperture Z-scan technique according to previously described method.²⁴ Two-photon excited fluorescence (2PF) was excited by the fs pulses with different intensities at wavelength of 800 nm. The repetition rate of the laser pulses is 250 kHz and the pulse duration is 80 fs. The measurement was performed with a fixed scattering angle of 90°. The size of the nanoparticles was determined by an ALV-5000 laser light scattering spectrometer (DLS). The SEM micrographs were obtained on a JEOL JSM-6360 scanning electron microscope (SEM). The cell imaging experiments were carried out with an Olympus FV1000 laser scanning confocal microscope and a 60 X oilimmersion objective lens.

Synthesis

(4-(4,6-Di-*p*-tolyl-1,3,5-triazin-2-yl)benzyl)dimethylphosphine Oxide (4)

In a 100 mL round-bottom flask, 2, 4, 6-tri(*p*-tolyl)-1, 3, 5-triazine (3 g, 8.5 mmol), *N*-bromobutanamide (NBS) (1.5 g, 8 mmol), and benzoyl peroxide (BPO) (0.3 g, 1.2 mmol) were dissolved into 50 mL of chlorobenzene and heated at 110 °C for 7

h. The mixture was filtered, and the solvent was removed under vacuum. The residue was dissolved into trimethyl phosphite (10 mL) and refluxed for 9 h. The excessive trimethyl phosphite was removed under vacuum. The residue was purified by column chromatography on silica (DCM) to afford the product as a white powder (2 g, yield: 55%). ¹H NMR (CDCl₃, 400 MHz), δ: 8.72 (d, *J* = 7.7 Hz, 2 H), 8.65 (d, *J* = 8.2 Hz, 4 H), 7.50 (dd, *J* = 8.4, *J* = 2.4 Hz, 2 H), 7.37 (d, *J* = 8.0 Hz, 4 H), 3.73 (d, *J* = 3.3 Hz, 6 H), 3.30 (d, *J* = 22.1 Hz, 2 H), 2.48 (s, 6 H). ¹³C NMR (CDCl₃, 100 MHz), δ: 171.43, 170.98, 143.01, 133.52, 132.80, 129.87, 129.34, 129.18, 128.89, 128.24, 52.34, 33.73, 29.60. MS (EI) (*m/z*): [(M+H)⁺] Calcd for C₂₆H₂₆N₃O₃P, 460.2; found: 460.1.

(((6-(p-Tolyl)-1,3,5-triazine-2,4-diyl)bis(4,1-phenylene))bis(methylene))bis(dimethylphosphine oxide) (5)

In a 100 mL round-bottom flask, 2,4,6-tri(p-tolyl)-1,3,5-triazine (3 g, 8.5 mmol), NBS (3 g, 16 mmol) and BPO (0.3 g, 1.2 mmol) were dissolved into 50 mL of chlorobenzene and heated at 110 °C for 7 h. The mixture was filtered and the solvent was removed under vacuum. The residue was dissolved into trimethyl phosphite (10 mL) and refluxed for 9 h. The excessive trimethyl phosphite was removed under vacuum. The residue was purified by column chromatography on silica (DCM) to afford the product as a white powder (2.3 g, yield: 53%). ¹H NMR (CDCl₃, 400 MHz), δ: 8.72 (d, *J* = 7.9 Hz, 4 H), 8.65 (d, *J* = 7.1 Hz, 2 H), 7.51 (d, *J* = 7.6 Hz, 4 H), 7.37 (d, *J* = 7.7 Hz, 2 H), 3.71 (d, *J* = 10.9 Hz, 12 H), 3.30 (d, *J* = 22.1 Hz, 4 H), 2.48 (s, 3 H). ¹³C NMR (CDCl₃, 100 MHz), δ: 171.48, 171.05, 143.16, 136.03, 135.93, 135.13, 133.37, 130.04, 129.20, 128.91, 53.09, 33.79, 32.42. MS (EI) (*m/z*): [(M+H)⁺] Calcd for C₂₈H₃₁N₃O₆P₂, 568.5; found: 568.1.

(4,4',4''-(1,3,5-Triazine-2,4,6-triyl)tris(benzene-4,1-diyl)tris(methylene)triphosphonate (6)

In a 100 mL round-bottom flask, 2,4,6-Tri(p-tolyl)-1,3,5-triazine (3.51 g, 10 mol), NBS (5.34 g 30 mmol) and BPO (0.3 g, 1.2 mmol) were dissolved into 50 mL chlorobenzene and heated at 110 °C for 7 h. The mixture was filtered and the solvent was removed under vacuum. The residue was dissolved into trimethyl phosphite (10 mL) and refluxed for 9 h. The excessive trimethyl phosphite was removed under vacuum. The residue was purified by column chromatography on silica (ethanol: DCM = 1:10, v/v) to afford the product as a white powder (5.3 g, yield: 78 %). ¹H NMR (CDCl₃, 400 MHz), δ: 8.71 (d, *J* = 8.0 Hz, 6 H), 7.51 (m, 6 H), 3.61 (d, *J* = 10.8 Hz, 18 H), 3.30 (d, *J* = 22.0 Hz, 6 H). ¹³C NMR (CDCl₃, 100 MHz), δ: 171.3, 136.3, 136.2, 135.0, 135.0, 130.1, 130.1, 129.3, 129.2, 53.1, 53.0, 33.9, 32.5. HRMS (EI) (*m/z*): [M⁺] Calcd for C₃₀H₃₆N₃O₉P₃, 675.1664; found: 675.1663.

4-[N,N-Bis(4-iodophenyl)amino]benzaldehyde (7)

A modified version of a previously reported method was used. In a 500 mL three-necked round-bottom flask, 4-(*N,N*-diphenylamino)benzaldehyde (14.00 g, 51.28 mmol), potassium iodide (11.43 g, 68.85 mmol), acetic acid (210 mL) and water (20 mL) were heated to 80 °C. After stirring for 1 h, potassium iodate (10.97 g, 51.26 mmol) was added and the reaction was stirred at 80 °C for 4 h. The solution was allowed to cool and the solid was collected, washed with water and recrystallized from DCM/ethanol (1: 5, v/v) giving the product as a yellow powder (20.05 g, yield: 75%). ¹H NMR (CDCl₃, 400 MHz), δ: 9.89 (s, 1

H), 7.75 (d, *J* = 9.0 Hz, 2 H), 7.67 (d, *J* = 9.0 Hz, 4 H), 7.09 (d, *J* = 9.0 Hz, 2 H), 6.93 (d, *J* = 9.0 Hz, 4 H).

4-(bis(4-(bis(4-(2,2,3,3-tetramethylbutyl)phenyl)amino)phenyl)amino)benzaldehyde (8)

A modified version of a previously reported method was used. In a 250 mL round-bottom flask, 4-[*N,N*-di(4-iodophenyl)amino]benzaldehyde (3 g, 5.7 mmol) bis-(4-(2, 2, 3, 3-tetramethylbutyl)phenyl)amine (6 g, 17.1 mmol), potassium carbonate (6.76 g, 49.02 mmol), activated copper bronze (1.6 g, 25.7 mmol) and 18-crown-6 (0.11 g, 0.042 mmol) were refluxed in 1, 2-dichlorobenzene (100 mL) for 48 h under argon atmosphere. The mixture was filtered and the solvent was removed under vacuum. The residue was purified by column chromatography on silica (petroleum ether (PE) : DCM = 1:1, v/v) to afford the product as a yellow powder (2 g, yield: 34%). ¹H NMR (DMSO-*d*₆, 400 MHz), δ: 9.73 (s, 1 H), 7.69 (d, *J* = 8.9 Hz, 2 H), 7.33 (d, *J* = 8.6 Hz, 8 H), 7.12 (d, *J* = 8.9 Hz, 4 H), 6.97 (d, *J* = 8.6 Hz, 8 H), 6.91 (d, *J* = 8.8 Hz, 4 H), 6.83 (d, *J* = 8.8 Hz, 2 H), 1.71 (s, 8 H), 1.55 (s, 24 H), 0.75 (s, 36 H). ¹³C NMR (THF-*d*₈, 126 MHz), δ: 189.21, 154.12, 146.13, 145.62, 145.18, 140.37, 139.25, 131.29, 127.78, 127.62, 124.40, 124.09, 118.29, 57.52, 38.60, 32.74, 31.86, 31.62. HRMS (ESI) (*m/z*): [(M+H)⁺] calcd for C₇₅H₉₇N₃O, 1056.7632; found: 1056.6593.

(E)-N1-(4-(bis(4-(2,2,3,3-tetramethylbutyl)phenyl)amino)phenyl)-N1-(4-(4-(4,6-di-p-tolyl-1,3,5-triazin-2-yl)styryl)phenyl)-N4,N4-bis(4-(2,2,3,3-tetramethylbutyl)phenyl)

benzene-1,4-diamine (ATT-1)
In a 100 mL round-bottom flask were added **4** (150 mg, 0.32 mmol), **8** (400 mg, 0.38 mmol), potassium tert-butoxide (230 mg, 1.8 mmol), 18-crown-6 (20 mg, 0.08 mmol) and 50 mL dichloromethane under argon atmosphere. After stirring at 45 °C for 6 h, the mixture was pour into distilled water and extracted with dichloromethane and water. The combined organic phases were dried over anhydrous MgSO₄ and concentrated using a rotary evaporator. The residue was purified by column chromatography on silica (PE : DCM = 4:1, v/v) the product as a yellow powder (160mg, yield: 33%). ¹H NMR (THF-*d*₈, 400 MHz), δ: 8.63 (d, *J* = 8.2 Hz, 2 H), 8.56 (d, *J* = 8.0 Hz, 4 H), 7.60 (d, *J* = 7.9 Hz, 2 H), 7.36 (d, *J* = 7.8 Hz, 2 H), 7.27 (d, *J* = 7.8 Hz, 4 H), 7.16 (d, *J* = 8.2 Hz, 8 H), 6.87 (dd, *J* = 14.4 Hz, 7.9 Hz, 20 H), 3.47 (s, 6 H), 2.41 (s, 8 H), 1.25 (s, 24 H), 0.66 (s, 36 H). ¹³C NMR (THF-*d*₈, 100 MHz), δ: 171.32, 171.04, 145.21, 143.98, 143.81, 142.89, 142.32, 141.72, 134.78, 133.75, 130.47, 129.10, 128.76, 127.67, 126.84, 126.15, 125.53, 124.12, 123.28, 121.63, 32.08, 31.22, 31.01, 24.55, 24.35, 24.15. HRMS (ESI) (*m/z*): [M⁺] calcd for C₉₉H₁₁₆N₆: 1389.9295; found: 1389.9337.

[2,4-tris((4-(*N,N*-Bis(4-(*N,N*-bis(4-tert-octylphenyl)amino)phenylamino)(benzene-4,1-diyl)(ethene-2,1-diyl)(benzene-4,1-diyl))-6-p-toluene]-1,3,5-triazine (ATT-2)

In a 100 mL round-bottom flask were added **5** (150 mg, 0.26 mmol), **8** (700 mg, 0.66 mmol), potassium tert-butoxide (230 mg, 1.8 mmol), 18-crown-6 (20 mg, 0.08 mmol) and 50 mL dichloromethane under argon atmosphere. After stirring at 45 °C for 6 h, the mixture was poured into distilled water and extracted with DCM and water. The combined organic phases were dried over anhydrous MgSO₄ and concentrated using a rotary evaporator. The residue was purified by column chromatography on silica (PE : DCM = 4:1, v/v) the product as a yellow powder

(200 mg, yield: 23%). ¹H NMR (THF-*d*₈, 400 MHz), δ: 8.66 (d, *J* = 8.3 Hz, 4 H), 8.59 (d, *J* = 8.1 Hz, 2 H), 7.63 (d, *J* = 8.1 Hz, 4 H), 7.38 (s, 4 H), 7.29 (d, *J* = 8.1 Hz, 2 H), 7.14 (t, *J* = 20.9 Hz, 19 H), 7.04 – 6.56 (m, 40 H), 2.36 (s, 3 H), 1.65 (s, 16 H), 1.26 (s, 48 H), 0.66 (s, 72 H). ¹³C NMR (THF-*d*₈, 100 MHz), δ: 170.89, 170.62, 147.74, 144.77, 143.53, 143.37, 142.53, 141.90, 141.20, 134.34, 133.28, 130.03, 129.98, 129.93, 128.70, 128.41, 127.18, 126.44, 125.77, 125.12, 125.06, 123.69, 122.86, 121.15, 30.81, 30.60, 24.14, 23.94, 23.74, 23.54. HRMS (ESI) (*m/z*): [*M*⁺] calcd for C₁₇₄H₂₁₁N₉: 2427.6821; found: 2427.6984.

2,4,6-tris[(4-(*N,N*-bis(4-(*N,N*-bis(4-*tert*-octylphenyl)amino)phenylamine)(benzene-4,1-diyl)(ethene-2,1-diyl)(benzene-4,1-diyl)]-1,3,5-triazine (ATT-3)

In a 100 mL round-bottom flask were added **6** (190 mg, 0.25 mmol), **8** (1.12 g, 1 mmol), potassium *tert*-butoxide (336 mg, 3.0 mmol), 18-crown-6 (20 mg, 0.08 mmol) and 50 mL dichloromethane under argon atmosphere. After stirring at 45 °C for 6 h, the mixture was poured into distilled water and extracted with dichloromethane and water. The combined organic phases were dried over anhydrous MgSO₄ and concentrated using a rotary evaporator. The residue was purified by column chromatography on silica (PE : DCM = 4:1, v/v) the product as a yellow powder. ¹H NMR (THF-*d*₈, 400 MHz), δ: 8.65 (d, *J* = 8.4 Hz, 6 H), 7.62 (d, *J* = 8.4 Hz, 6 H), 7.44 – 7.34 (m, 6 H), 7.26 – 7.01 (m, 30 H), 6.97 – 6.75 (m, 54 H), 1.63 (s, 24 H), 1.30 (s, 72 H), 0.66 (s, 108 H). ¹³C NMR (THF-*d*₈, 100 MHz), δ: 171.04, 145.20, 143.94, 143.79, 142.39, 141.62, 134.93, 130.58, 129.15, 127.61, 126.85, 126.20, 125.55, 124.12, 123.28, 121.56, 56.86, 37.90, 32.10, 31.24, 31.02. MALDI-TOF: [*M*⁺] Calcd for C₂₄₉H₃₀₆N₁₂, 3466.4381; found: 3466.4153.

Preparation of AIE nanoparticles

A solution of ATT-(1-3) in THF (30 μL, 1 mg/mL) was injected into 30 mL PBS buffer (pH = 7.4) under ultrasonication. THF was evaporated by N₂ flow at 70 °C, and the solution was followed by filtration through a 0.2 μm filter.

Live cell imaging

Hela Cells were plated on 14 mm glass coverslips and allowed to adhere for 12 h. The cells were washed with PBS and then incubated with ATT-(1-3), respectively, in PBS (pH 7.4) for 90 min at 37 °C. Cell imaging was then carried out after washing the cells with PBS.

Acknowledgements

This work was supported by NSFC/China (21372082, 2116110444, 21172073 and 91233207) and the National Basic Research 973 Program (2013CB733700 and 2013CB834701). We are grateful to Wen Lv from Nanjing University of Posts and Telecommunications for significant help.

Notes and references

^aKey Laboratory for Advanced Materials, Institute of Fine Chemicals and Department of Chemistry, East China University of Science and Technology, 130 Meilong Road, Shanghai, 200237, China. Fax: +86-21-64250940; Tel: +86-21-64250940; E-mail: jlhua@ecust.edu.cn; jcwu@ecust.edu.cn

^bDepartment of Chemistry & Laboratory of Advanced Materials, Fudan University, 220 Handan Road, Shanghai 200433, China
^cKey Laboratory of Polar Materials and Devices, Ministry of Education, East China Normal University, Shanghai 200241, China

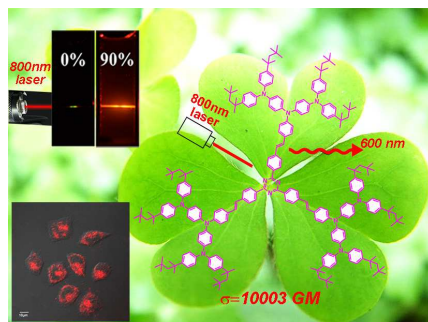
- (a) S. H. Guang, L. S. Tan, Q. D. Zheng and N. P. Paras. *Chem. Rev.*, 2008, **108**, 1245; (b) H. Y. Ahn HY, K. E. Fairfull-Smith and B. J. Morrow. *J. Am. Chem. Soc.*, 2012, **134**, 7297. (c) M. Maurin1, L. Vurth, J. Vial, P. Baldeck, S. R. Marder, B. V. Sanden, O. Stephan. *Nanotechnology*, 2009, **20**, 235102.
- (a) W. Denk, J. H. Strickler and W. W. Webb. *Science*, 1990, **248**, 73; (b) S. Yao, D. B. Kevin. *Eur. J. Org. Chem.*, 2012, **17**, 3199.
- (a) H. J. Kim, C. H. Heo, H. M. Kim. *J. Am. Chem. Soc.*, 2013, **135**, 17969; (b) B. D. G. Bordeau, E. F. Paul, F. Mahuteau-Betzer, N. Saettel, G. Metge, C. Fiorini-Debuisschert, F. Charra, M. P. Teulade-Fichou. *J. Am. Chem. Soc.*, 2013, **135**, 12697.
- (a) S. Sumalekshmy, J. F. Christoph. *Chem. Mater.*, 2011, **23**, 483; (b) V. Hrobarikova, P. Hrobarik, P. Gajdos, I. Fitisil, M. Fakis, P. Persephonis, P. Zahradnik. *J. Org. Chem.*, 2010, **75**, 3053.
- M. Pawlicki, H. A. Collins, R. G. Denning, H. L. Anderson. *Angew. Chem. Int. Ed.*, 2009, **48**, 3244.
- (a) D. Blaise, B. Guillaume, F. P. Elodie, M. B. Florence, S. Nicolas, M. Germain, F. D. Céline, C. Fabrice, T. F. Marie-Paule. *J. Am. Chem. Soc.*, 2013, **135**, 12697; (b) R. Cedric, L. D. Celine, M. Yohan, C. Sophie, M. Olivier, M. Emmanuel, B. D. Mireille. *Chem. Eur. J.*, 2012, **18**, 12487.
- T. C. Lin, Y. H. Lee, C. Y. Liu, B. R. Huang, M. Y. Tsai, Y. J. Huang, J. H. Lin, Y. K. Shen, C. Y. Wu. *Chem. Eur. J.*, 2013, **19**, 749.
- J. Luo, Z. Xie, J. W. Y. Lam, L. Cheng, H. Chen, C. Qiu, H. S. Kwok, X. Zhan, Y. Liu, D. Zhu, B. Z. Tang. *Chem. Commun.*, 2001, **21**, 1740.
- Y. Hong, J. W. Y. Lam, B. Z. Tang. *Chem. Commun.*, 2009, **29**, 4332.
- Z. Wang, S. Chen, J. W. Y. Lam, W. Qin, R. T. K. Kwok, N. Xie, X. Hu, B. Z. Tang. *J. Am. Chem. Soc.*, 2013, **135**, 8238.
- (a) X. G. Gu, G. X. Zhang, D. Q. Zhang. *Analyst*, 2012, **137**, 365; (b) S. Chen, Y. Hong, Y. Liu, J. Liu, C. W. T. Leung, M. Li, R. T. K. Kwok, E. Zhao, J. W. Y. Lam, Y. Yu, B. Z. Tang. *J. Am. Chem. Soc.*, 2013, **135**, 4926; (c) Y. Hong, L. Meng, S. Chen, C. W. T. Leung, M. Faisal, D. A. Silva, J. Liu, J. W. Y. Lam, B. Z. Tang. *J. Am. Chem. Soc.*, 2012, **134**, 1680.
- Z. Chi, X. Zhang, B. Xu, X. Zhou, C. Ma, Y. Zhang, S. Liu, J. Xu. *Chem. Soc. Rev.*, 2012, **41**, 3878.
- (a) T. Tian, X. Chen, H. Li, Y. Wang, L. Guo, L. Jiang. *Analyst*, 2013, **138**, 991; (b) B. Xu, M. Xie, J. He, B. Xu, Z. Chi, J. W. Tian, L. Jiang, F. Zhao, S. Liu, Y. Zhang, Z. Xu, J. Xu. *Chem. Commun.*, 2013, **49**, 273; (c) Y. Yuan, T. K. Ryan, B. Z. Tang, B. Liu. *J. Am. Chem. Soc.*, 2014, **136**, 2546.
- (a) Y. H. Jiang, Y. C. Wang, J. L. Hua, J. Tang, B. Li, S. X. Qian, H. Tian. *Chem. Commun.*, 2010, **46**, 4689; (b) K. Li, Y. H. Jiang, D. Ding, X. Zhang, Y. Liu, J. L. Hua, S. S. Feng, B. Liu. *Chem. Commun.*, 2011, **47**, 7323.
- (a) S. H. Guang, L. S. Tan, Q. D. Zheng, N. P. Paras. *Chem. Rev.*, 2008, **108**, 1245; (b) H. Y. Ahn HY, K. E. Fairfull-Smith, B. J. Morrow. *J. Am. Chem. Soc.*, 2012, **134**, 7297. (c) M. Maurin1, L. Vurth, J. Vial, P. Baldeck, S. R. Marder, B. V. Sanden, O. Stephan. *Nanotechnology*, 2009, **20**, 235102.
- C. Liu, K. C. Tang, H. Zhang, H. A. Pan, J. L. Hua, B. Li, P. T. Chou. *J. Phys. Chem. A*, 2012, **116**, 12339.
- (a) X. Y. Shen, W. Z. Yuan, Y. Liu, Q. Zhao, P. Lu, Y. Ma, I. D. Williams, A. Qin, J. Z. Sun, B. Z. Tang. *J. Phys. Chem. C*, 2012, **116**, 10541; (b) W. Qin, D. Ding, J. Liu, W. Z. Yuan, Y. Hu, B. Liu, B. Z. Tang. *Adv. Funct. Mater.*, 2012, **22**, 771.
- S. J. K. Pond, M. Rumi, M. D. Levin, T. C. Parker, D. Beljonne, M. W. Day, J.-L. Brédas, S. R. Marder, J. W. Perry. *J. Phys. Chem. A*, 2002, **106**, 11470.
- B. Z. Tang, Y. Geng, J. W. Y. Lam, B. Li, X. Jing, X. Wang, F. Wang, A. B. Pakhomov, X. Zhang. *Chem. Mater.*, 1999, **11**, 1581.

-
- 20 (a) Y. Ren, J. W. Y. Lam, Y. Dong, B. Z. Tang, K. S. Wong. *J. Phys. Chem. B*, 2005, **109**, 1135; (b) Y. Ren, Y. Dong, J. W. Y. Lam, B. Z. Tang, K. S. Wong. *Chem. Phys. Lett.*, 2005, **402**, 468.
- 21 S. H. Guang, L. S. Tan, Q. D. Zheng, N. P. Paras. *Chem. Rev.*, 2008, **108**, 1245.
- 5 22 Y. T. Gao, H. Zhang, T. Jiang, J. Yang, B. LI, Z. LI, J. L. Hua. *Sci. China. Chem.*, 2013, **56**, 1204.
- 23 W. Guan, X. H. Zhang, J. Geng, L. Kai, D. Dan, P. K. Y. Pu, L. Cai, Y. H. Lai, B. Liu. *Chem. Eur. J.*, 2012, **18**, 9705.
- 10 24 Z. J. Ning, Z. Chen, Q. Zhang, Y. L. Yan, S. X. Qian, Y. Cao, H. Tian. *Adv. Funct. Mater.*, 2007, **17**, 3799.
- 25 Y. H. Jiang, Y. C. Wang, J. L. Hua, S. Y. Qu, S. Q. Qian, H. Tian. *J. Polym. Sci., Part A*, 2009, **47**, 4400.
- 15 26 N. B. McKeown, S. Badriya, M. Helliwell, M. Shkunov. *J. Mater. Chem.*, 2007, **17**, 2088.

Graphical Abstract

Alkyl-triphenylamine End-capped Triazines with AIE and Large Two-photon Absorption Cross-sections for Bioimaging

Yuting Gao^a, Yi Qu^b, Tao Jiang^a, Hao Zhang^a, Nannan He^a, Bo Li^c, Junchen Wu^{a*}, and Jianli Hua^{a*}



Three alkyl-triphenylamine end-capped triazines (**ATT-1-3**) with AIE were synthesized and two-photon absorption cross sections of **ATT-3** was 10003 GM.